Biomedicine & Pharmacotherapy 160 (2023) 114320

Contents lists available at ScienceDirect

Biomedicine & Pharmacotherapy

journal homepage: www.elsevier.com/locate/biopha

Bias-force guided simulations combined with experimental validations towards GPR17 modulators identification

Sana Kari [a], Akshaya Murugesan [a], Ramesh Thiyagarajan [b], Srivatsan Kidambi [c], Jamoliddin Razzokov [d,e,f,g,h,1], Chandrabose Selvaraj [i,2], Meenakshisundaram Kandhavelu [a,*,3], Parthiban Marimuthu [j,*,4]

[a] Molecular Signaling Group, Faculty of Medicine and Health Technology, Tampere University and BioMediTech, P.O.Box 553, 33101 Tampere, Finland
[b] Department of Basic Medical Sciences, College of Medicine, Prince Sattam Bin Abdulaziz University, Al-Kharj 11942, Kingdom of Saudi Arabia
[c] Department of Chemical and Biomolecular Engineering, University of Nebraska-Lincoln, 820 N 16th Street, 207 Othmer Hall, NE 68588, USA
[d] Institute of Fundamental and Applied Research, National Research University TIIAME, Kori Niyoziy 39, 100000 Tashkent, Uzbekistan
[e] College of Engineering, Akfa University, Milliy Bog Street 264, 111221 Tashkent, Uzbekistan
[f] Institute of Material Sciences, Academy of Sciences, Chingiz Aytmatov 2b, 100084 Tashkent, Uzbekistan
[g] Department of Physics, National University of Uzbekistan, Universitet 4, 100174 Tashkent, Uzbekistan
[h] Laboratory of Experimental Biophysics, Centre for Advanced Technologies, Universitet 7, 100174 Tashkent, Uzbekistan
[i] Department of Biotechnology, Division of Research and Innovation, Saveetha School of Engineering, SIMATS, Chennai 602105, Tamil Nadu, India
[j] Pharmaceutical Science Laboratory (PSL – Pharmacy) and Structural Bioinformatics Laboratory (SBL – Biochemistry), Faculty of Science and Engineering, Åbo Akademi University, FI-20520 Turku, Finland

ARTICLE INFO

Keywords:
GPR17
Orphan-GPCRs
Remyelination
Bias-force simulation
Forskolin-stimulated cAMP accumulation

ABSTRACT

Glioblastoma Multiforme (GBM) is known to be by far the most aggressive brain tumor to affect adults. The median survival rate of GBM patient's is < 15 months, while the GBM cells aggressively develop resistance to chemo- and radiotherapy with their self-renewal capacity which suggests the pressing need to develop novel preventative measures. We have recently proved that GPR17 —an orphan G protein-coupled receptor— is highly expressed on the GBM cell surface and it has a vital role to play in the disease progression. Despite the progress made on GBM downregulation, there still remain difficulties in developing a promising modulator for GPR17, till date. Here, we have performed robust virtual screening combined with biased-force pulling molecular dynamic (MD) simulations to predict high-affinity GPR17 modulators followed by experimental validation. Initially, the database containing 1379 FDA-approved drugs were screened against the orthosteric binding pocket of the GPR17. The external bias-potentials were then applied to the screened hits during the MD simulations which enabled to predict a spectrum of rupture peak force values that were used to select four approved drugs –ZINC000003792417 (Sacubitril), ZINC000014210457 (Victrelis), ZINC000001536109 (Pralatrexate) and ZINC000003925861 (Vorapaxar)– as top hits. The hits selected turns out to demonstrate unique dissociation pathways, interaction pattern, and change in polar network over time. Subsequently the selected hits with GPR17 were measured by inhibiting the forskolin-stimulated cAMP accumulation in GBM cell lines, LN229 and SNB19. The *ex vivo* validations shows that Sacubitril drug can act as a full agonist, while Vorapaxar functions as a partial agonist for GPR17. The pEC_{50} of Sacubitril was identified as 4.841 and 4.661 for LN229 and SNB19, respectively. Small interference of the RNA (siRNA)– silenced the GPR17 to further validate the targeted binding of Sacubitril with GPR17. In the current investigation, we have identified new repurposable GPR17 specific drugs which are likely to increase the opportunity to treat orphan deadly diseases.

* Corresponding authors.
E-mail addresses: meenakshisundaram.kandhavelu@tuni.fi (M. Kandhavelu), parthiban.marimuthu@abo.fi (P. Marimuthu).
[1] https://orcid.org/0000-0002-3098-0797
[2] https://orcid.org/0000-0002-8115-0486
[3] https://orcid.org/0000-0002-4986-055X
[4] https://orcid.org/0000-0003-4960-2160

https://doi.org/10.1016/j.biopha.2023.114320
Received 10 December 2022; Received in revised form 17 January 2023; Accepted 26 January 2023
Available online 28 January 2023

1. Introduction

G-protein coupled receptors (GPCRs) are a large family of receptors which are involved in intracellular signaling. Among the several GPCRs, GPR17 plays a vital role in many neurological diseases including glioblastoma, astrocytoma, oligodendroglioma, multiple sclerosis, Alzheimer, Parkinson's [1,2]. Therefore, GPR17 has been recognized as a potential target for developing novel therapeutics for neurological diseases. Recently, we have used high throughput computational approach integrated with experimental validation for finding novel ligands from the chemical compounds of PubChem database. Among several thousands of compounds, we have found a novel agonist, T0510.3657, with the anti-GBM potential [3]. However, the conventional methods towards novel drug identification typically takes more than a decade to obtain FDA approval because of stringent regulations combined with high costs which can be facilitated through drug repurposing process. This can in turn lead to an increase in efficiency of the therapies, particularly for rare diseases [4].

The drug repurposing [5] (a.k.a. drug repositioning, drug reprofiling, drug redirecting or drug rediscovery or drug reprofiling) is a process of leveraging an existing drug (Remdesivir is a broad-spectrum antiviral medicine) to treat newly emerged Remdesivir (approved to treat Covid19 in emergency purpose by FDA [6]), unknown or orphaned disease. Considering the pressing need to treat patients with newly emerging disease within a short period of time, the repurposed drugs are seen as an alternative and beneficial way of treatment. [7,8]. This approach is a familiar multi-step process that is widely performed based on identification of *(i)* pathological target, *(ii)* potential lead candidate, *(iii)* thorough investigation of the target-lead binding mechanism, *(iv)* multiple stages of preclinical investigations, and *(v)* filing marketing approval [9]. Generally, a certified drug is likely to have multiple therapeutic applications, i.e., a single drug can interact with multiple targets and indeed expresses various downstream signaling [10]. Likewise, a molecular target associated with a specific pathological process could disrupt other normal biological processes by causing some side effects [11]. Furthermore, repurposing the existing drugs formulation could also serve as a viable alternative to treat emerging disease, when the straightforward repurposing strategy exhibited an unprecedented failure [7]. Considering these facts, the drug repurposing process must be carefully performed to avoid negative effects. However, this powerful technique requires thorough knowledge of biological and molecular pathways that a drug can modulate as well as interact with, the risks can be significantly diminished, resulting in successful repurposing of a drug. Thus, the process of drug repurposing has its own nuances towards modern drug discovery [12].

To combat the effects of the glioblastoma disease in a rapid phase, the conventional steps towards identification of novel potential drug candidates and performing subsequent multiple clinical trials is a time-consuming process. Deploying the advanced computational strategies to repurpose pre-approved drugs towards specific pharmacological target could significantly accelerate the novel drug identification process [9, 13–17]. The advanced computational techniques associated with state-of-the-art tools can aid (i) identification of novel drugs that could specifically bind to the pathological target [18,19], (ii) elucidate the mechanistic assessment of various drugs recognizing the pathological target [20] (iii) thermodynamics of drugs binding (M^{Pro} - [21]). Application of the computational approach in combination with other advanced cutting-edge methods has shown reliable evidence towards successful repurposing [20,22,23]. For instance, *Hatzimouratidis K* identified Sildenafil [24], a drug identified for erectile dysfunction, later repurposed for the treatment of hypertension. Similarly, *Merten N* et al., has identified HAMI3379 [25] as a potential inhibitor for GPR17 across various cellular backgrounds, that had originally been developed to treat cardiovascular and inflammatory disorders, which is also known to inhibit cysteinyl-leukotriene CysLT2 receptor. Similarly, *Morselli* et al. employed AI network-based drug repurposing approach and predicted multiple potential drugs that could be directly repurposed to treat COVID-19 and regulate the overstimulated immune system that showed their advantages over docking-based identification methods [26]. *Ma, C* et al. spotted the FDA-approved protease inhibitors Boceprevir, GC-376, and calpain inhibitors II, XII as a validated antiviral drug for SARS-CoV and MERS-CoV using FRET-based enzymatic assay and drug repurposing screening strategy [6]. Later, we leveraged the binding affinity details from this study and attempted to further explore the mechanistic basis of protease inhibitors by binding to M^{pro} using advanced multiple computational approaches such as docking, long-range MD simulations. In addition to this approach, the estimation of the binding free-energy (BFE) for each drug was also computed in detail, which in turn provided deep insights into the drug-target binding [21]. Overall, the drug repurposing approach not only provides pre-approved drugs for orphan and emerging diseases in a short period of time, but also provides a novel method to explore the utility of discontinued and underutilized drugs to elaborate new medical applications [27,28].

The current study is an attempt to leverage the popular *drug repurposing* technique aimed at expediting the finding of novel/pre-approved drugs to treat patients suffering from GBM disease progression in a short period of time. Here, the initial investigations were carried out using multiple advanced computational techniques, such as homology modeling and the high-throughput virtual screening (HTVS; Schrödinger Release 2021–2, Schrödinger, LLC, New York, NY, 2021) of FDA-approved database, which altogether make up the multistate simulations, i.e., the MD simulations and biased-force/steered MD simulations. The biased-force MD simulations were used to reduce the hit compounds identified by HTVS and uncover the list of the specific compounds that demonstrate a tight binding with the GPR17 model together with drug dissociation pathways. Next, the drugs that were identified based on previous *insilico* approaches were subjected to in vitro validation in GBM cells. Overall, the results of the current study might provide crucial evidence for novel, readily usable drugs combined with its regulatory mechanism to modulate the GPR17, which in turn might impede the progression of GBM disease.

2. Materials and methods

2.1. Homology modeling of GPR17

The 3D structure of ligand bound conformation of GPR17 is not available till-date. Recently, a Cryo-EM structure of long-isoform of GPR17 was determined with inhibitory G-protein bound conformation [29]. Therefore, the structure is not usable for ligand screening due to the pocket occupied by EC loop 2. However, the current study aims to use short isoform of GPR17 in its native state suitable for drug screening studies while the orthosteric binding pocket of the recently determined structure was occupied with EC loop 2. For these reasons the existing GPR17-Gi complex is unapplicable for our investigations. The initial attempts thus have been made to build up a homology model of GPR17. First, the primary sequence for GPR17 was obtained from the UniProt DB (ID: Q13304) [30]. The NCBI-BlastP [31] was used to select the template structure corresponding to the GPR17 sequence against PDB. The top hit was selected based on the sequence identity and query coverages (in %), respectively. Subsequently, the online Clustal-Omega [32] was used to generate initial primary sequence alignment for the template and the target, while the standalone Jalview v2.11.1.3 [33,34] was used to manually curate the appropriate 7-TM spanning α-helical segments. Finally, the resulting pairwise alignment was subjected to the Modeller 9.20 v [35] program to generate individual conformations of the GPR17 models, embedded with the crystal ligand (ONO-2570366 [36]; used as a reference ligand for a later analysis) in its original conformational state. Here, the GPR17 model was developed complexed with x-ray ligand to apply the straightforward grid preparation method during the subsequent docking investigation, due to the high similarity in structural topology.

2.2. Refinement of GPR17 model

For the docking purpose, the representative model –GPR17 complexed with crystal ligand– from the homology modeling process was selected and subjected to automated refined process using "protein preparation wizard" (Protein Preparation Wizard; Epik, Schrodinger Inc., NY, USA, 2021.4) that assigns bond orders and polar hydrogens. Additionally, the protonation state of the charged residues (Asp, Glu, Arg, Lys and His) in the receptor molecule was generated using the inbuilt PROPKA program. Finally, the resulting protein-ligand complex was then thoroughly energy minimized using the optimized potentials for liquid simulations (OPLS4) force field [37], by applying the physiological pH using Epik [38,39].

2.3. Data acquisition, ligand database preparation and docking

In order to obtain the potential GPR17 modulators in a short period of time, employing the drug repurposing approach on the pre-approved drugs together with the advanced insilico methods is a valid and robust strategy due to its proven success rate of drugs identification [40]. Therefore, a database of the FDA-approved drug compounds (https://zinc.docking.org/substances/subsets/fda/; with 1379 molecules) obtained from the ZincDB was subjected to the LigPrep module in Maestro 2021–1, which adds any missing hydrogen atoms in ligands, assigns formal charges, generates a set of plausible poses based on ionization and tautomeric states, all of which were converted to 3D models at pH neutral using the all-atom OPLS4 force field. The resulting subset of DB with **5936** conformers were subjected to the virtual screening protocol using the "HTVS precision" present in the "Ligand Docking" panel. For this purpose the grid was generated using "Receptor Grid Generation" protocol by engaging the crystal ligand in "Pick to identify the ligand" option. The other options such as, sampling nitrogen inversions, ring conformations, all predefined functional groups and addition of Epik state penalties to the docking score were also used during the HTVS process, followed by XP docking to obtain the best hit compounds. Finally, the output from the XP docking was subjected to prime-MMGBSA [41] calculations to identify the binding free energy (kcal/mol).

2.4. Preparation of simulation systems

All the selected hit compounds and ONO-2570366 complexed with the GPR17 were used to build up independent simulation systems using the Charmm-GUI [42] (https://www.charmm-gui.org/) web-based platform. The parameters for all 17 (16 hits plus 1 crystal ligand) compounds were generated using the "Ligand Reader and Modeller" panel, while the POPC-only lipid model (126 ×125 in upper and lower leaflet) was used to completely pack the 7TM segments of GPR17 using the fully automated "membrane-bilayer builder" panel with CHARMM36m [43] force field. All the systems were solvated using the TIP3P water model [44], while the unbalanced charges were neutralized by NA^{+} and CL^{-} ions. Before the production runs, all the systems were subjected to six-steps equilibration runs, determined to gradually decrease the restrained forces on GPR17 and POPC bilayer. Finally, all systems were submitted to the restrain-free 100 ns equilibration runs using GROMACS [45] package. The Partial Mesh Ewald (PME) [46] and V-rescale [47] methods were used to monitor the long-range electrostatics and temperature coupling at 310 K, respectively. The Parrinello-Rahman [48] barostat with reference pressure of 1 bar and compressibility of 4.5×10^{-5} /bar was applied for pressure control. All covalent bonds were constrained to their equilibrium length by the LINCS algorithm [49].

2.5. Preparation of Bias-force Simulation systems

In order to obtain the binding strength between the hit compounds and binding site residues of GPR17, the bias-force pulling simulation technique was employed [50]. Here, the coordinates obtained from the final time period of the production run were used as an initial coordinate for the pulling simulations. In order to probe a constant dissociation pathway for a binding partner in a macromolecular complex, conventionally, the heavy atoms of the receptor will be restrained to a fixed position, while the center-of-mass of the whole or a specific atom of the binding partner will be subjected to the external bias-potential at a constant velocity (v). In the current study, the restrain force was set to all the Cα atoms of the GPR17, while a range of bias-potentials (constant velocity (v); v= 0.001–0.01 nm/ps and spring constant (k), k = 200–500 kJ/mol/nm2) were applied on the specific atom of the ligand coordinates on each complex for gradual dissociation from the receptor binding pocket along z axis. Finally, each complex was subjected to 4 ns simulation by applying the aforementioned bias-potentials, while the output frames were recorded at every 1 ps. All the trajectory outputs were used to estimate the total force (F) required for the complete dissociation of the ligand from the GPR17 binding pocket.

2.6. Simulation visualization and analysis

All MD trajectories were graphically visualized using VMD [51] and PyMol (www.pymol.org), and were also post-processed using GROMACS inbuilt programs. The simulation trajectory outputs were plotted using the GRACE software (http://plasma-gate.weizmann.ac.il/Grace/).

2.7. Experimental methods

Human glioblastoma (GBM) cell lines LN229 and SNB19 (obtained as a gift from Dr. Kirsi Granberg, Faculty of Medicine and Health Technology, Tampere. Finland) were used to test the efficacy of top repurposing drugs targeting GPR17 receptor protein. Originally, LN229 was derived from a right frontal parieto-occipital glioblastoma patient with the mutation on p52, p16, and p14ARF tumor suppressor genes while SNB19 was obtained from a left parieto-occipital glioblastoma patient. Both LN229 and SNB19 cells also over express GPR17 protein. These cell lines were cultured and maintained in Dulbecco's modified Eagle's medium (DMEM) (D5796, Sigma-Aldrich, USA) supplemented with 10% FBS (Biowest, France), 0.1 mg/mL streptomycin (Sigma-Aldrich, USA), 100 U/mL penicillin (Sigma-Aldrich, USA), and 0.025 mg/mL amphotericin B (Sigma-Aldrich, USA). The culture atmosphere was kept at 37 °C humidified with 5% CO_2(v/v).

2.8. Cyclic adenosine monophosphate (cAMP) measurements

LN229 and SNB19 cells were seeded in a white 96-well plate (NuclonThermoFisher Scientific, USA) with an initial density of 2×10^4 cells/well. After overnight incubation, the cells were washed with PBS. To increase the concentration of cAMP, cells were then induced with 10 μM Forskolin (F6886–10MG, Sigma-Aldrich, USA) at 37 °C for 15 min. Cells were then treated with increasing concentrations of 1, 10, 25, 50, 100 μM of top four repurposing drugs at 37 °C for 2 h. Cells were then assayed for measuring cAMP level using the cAMP-Glo Assay (V1501, Promega, USA) following the manufacturer's instructions. Briefly, the cells were loaded with 20 μL of cAMP Glo lysis buffer, followed by a shaking step of 30 min at RT. Then, the cells were incubated with the cAMP detection solution in 20 min, followed by incubation with the Kinase-Glo Reagent for 10 min at RT. The luminescence level of the control and the treated samples were measured using the Spark multimode microplate reader. The computer program GraphPad prism 9.0 software was used to generate dose-response curves (sigmoidal dose-response (variable slope) equation) and to calculate pEC_{50}. Standard error of mean (SEM) was calculated to present variation in data. The experiment was performed on both cell lines with three technical repeats of each sample.

2.9. RNA interference

LN229 and SNB19 cells with the confluence of 60–70% were transfected with 20 nM of pre-designed siRNA (Sense strand: GCGCAGACUGUUUAGGACUTT, Antisense strand: AGUCCUAAACAGUCUGCGCTC (AM16708 and #145193, Thermo Fisher) by Lipofectamine RNAiMAX Transfection Reagents (cat no. 13778030; Thermo Fisher Scientific, USA). After 48 hrs of transfection, cAMP Glo assay was performed by using kit protocol (V1501, Promega, USA) as described above. The luminescence level of the control and the drug treated samples were measured using the Tecan plate reader. The experiments were performed with three biological and technical repeats.

3. Results and discussion

3.1. Structural insights from the GPR17 model

An experimentally determined 3D structure towards the discovery of the novel GPR17 modulator isn't yet foolproof which could hinder the rational design of potential therapeutic agents. Therefore, the homology modeling technique was adapted, which is believed for a long time to seamlessly generate a 3D model of a protein of interest in a short time of period, when provided with the appropriate template. Taking this into account the primary sequence of GPR17 (swiss-prot: Q13304) was retrieved and directly queried using NCBI-BlastP against PDB. Based on the high percentage of identity (34.84%) and query coverage (76%), the crystal structure of the human cysteinyl leukotriene receptor 2 [36] ($CysLT_2$) in complex with ONO-2570366 (RCSB ID: 6RZ6; chain A; resolution 2.43 Å) was selected and used for the model building process by excluding the IC lysozyme segment (residue no: 1002–1106). Considering the fact that the GPR17 and $CysLT_2$ belong to the class A GPCR superfamily, which strongly shares the core 7TM α-helix molecular determinant, and its pharmacological profile, it is an appropriate choice to employ the selected template as a promising one. Subsequently, the model building process generated 50 energetically favorable GPR17 models. A representative GPR17 structure was then selected based on (i) higher DOPE scores generated by the Modeller program, (ii) structural superposition of all the models against the template structure and (iii) its individual lowest RMSD values using PyMol (The PyMOL Molecular Graphics System, Version 1.2r3pre, Schrödinger, LLC.).

Initially, to investigate the proper alignment of the molecular segments (Extracellular, EC; Transmembrane, TM; and the Intracellular, IC) between the representative and the template structure, the structural superposition was carried out using PyMol and was graphically investigated (Fig. 1b). The output displays that the selected model shows a good agreement with the template, i.e., (i) the core 7 TM segments, (ii) the IC loops and (iii) the highly conserved two disulphide linkages (51–297 and 132–209) that are present between the N-terminal loop and EC loop3, and EC2 and TM3 properly aligned, while the (iv) overall EC loop regions between the model and the template show just minor deviations, which is negligible.

Next, the binding site residues between the representative and the template structure were examined in the presence of the x-ray ligand (Fig. 1c). The binding site of the GPR17 model is surrounded by E54, E58, F62, Y140, Y144, Y148, V187, A190, M191, L194, L210, Q211, L212, R214, A217, H220, A221, V223, S224, V227, A228, R283, Y286, V287, N307 and R308 residues from all 7-TM domains and the EC2 loop regions. Among these residues, the crystal ligand interacts with Y140 residue by electrostatic interactions, and Y144 residue by π-π interactions. These interactions were also observed in the template structure. Finally, this well validated model was used as the initial coordinates for subsequent docking studies.

3.2. Screening the approved drugs

In order to identify a novel drug compound that could exhibit tight binding with GPR17, the *high-throughput virtual screening (HTVS)* strategy was implemented, due to its high feasibility and accuracy. Also, incorporating the "drug repurposing" approach targeting specific disease or a specific target of interest to the existing virtual screening method demonstrates several benefits over screening the generic databases, i.e., as the repurposed drug candidates have already gone through all crucial clinical trials and pharmacodynamics profiles during the previous investigations for its approval. Therefore, the repurposed drugs against GPR17 are believed to be highly promising that can yield novel candidates within a very short period of time with a cost-effective treatment of the glioblastoma disease.

3.3. Selection procedures for the screened compounds

Using the well pre-processed database of 5936 FDA-approved conformers, the HTVS campaign was deployed with the previously selected GPR17 model using Maestro. The hits selection was performed based on (i) docking scores generated with higher negative values and (ii) the binding modes of the drug compounds in comparison with the x-ray ligand together with its (iii) intramolecular interactions towards the target. Also, the structural investigation of the template ($CysLT_2R$) binding pocket demonstrates highly conserved key-anchoring tyrosine residue (Y119 in $CysLT_2R$) deep inside the binding pocket that plays a vital role in the ligand stabilization through multiple polar contacts [36].

Therefore, this criterion was also used as a crucial parameter for the hit selection (Fig. 2). Thus, in addition to the previously mentioned criteria, the novel drugs from the FDA-approved conformers that interacts with the tyrosine residue (Y140) situated in the corresponding position of GPR17 via polar contacts were also considered as hit compounds (Fig. 3). Based on this approach, the XP campaign initially yielded 1664 compounds as screened outputs.

Subsequently, in order to obtain hit compounds with enhanced binding specificity, it is essential to deeply investigate binding capacity of the screened compounds with its receptor particularly w.r.t its binding free-energy (BFE). In recent years the BFE estimation methods such as molecular mechanics generalized Born solvation accessibility (MMGBSA), free-energy perturbation (FEP), replica-exchange FEP (REFEP), thermodynamic integration (TI), metadynamics (MetaD), and potential mean-forces (PMF) are gaining much popularity due to its promising role in the identification of novel drugs. In the current investigation, the extensive energy evaluation method such as the prime-MMGBSA method that is available in Maestro was employed.

Subsequently, among the 1664 compounds from the HTVS campaign, top 16 hits (Figs. 3, 4 and Supplementary Fig. S1) were alone selected and subjected to the prime-MMGBSA method. This method estimates the total energy for the given complex from individual energy terms, such as, receptor, ligand and complex, respectively, [41] which is a highly reliable information for a novel drug discovery process. Later, to rank the best candidates, the cutoff value of − 30 was set to the prime-MMGBSA energy profile, which resulted in identification of 16 most-promising FDA-approved drug compounds (see Table 1) with a wide-range of scaffolds comprising amide, acetyl and aromatic groups. All these compounds were used for further analysis.

3.4. MD simulations

As the molecular mechanism of binding and the interaction of compounds obtained through the XP protocol (Table 1) are not well understood, all the screened plus the xray compounds complexed with GPR17 were initially subjected to classical molecular dynamics (MD) simulations. Here, the simulation systems were built individually, i.e., the FDA-approved screened compounds complexed with the GPR17 were properly embedded in the membrane (monounsaturated 1-palmitoyl-2-oleoyl-*sn*-glycero-3-phosphocholine - POPC) environment using the automated CHARMM-GUI protocol by applying CHARMM36 force

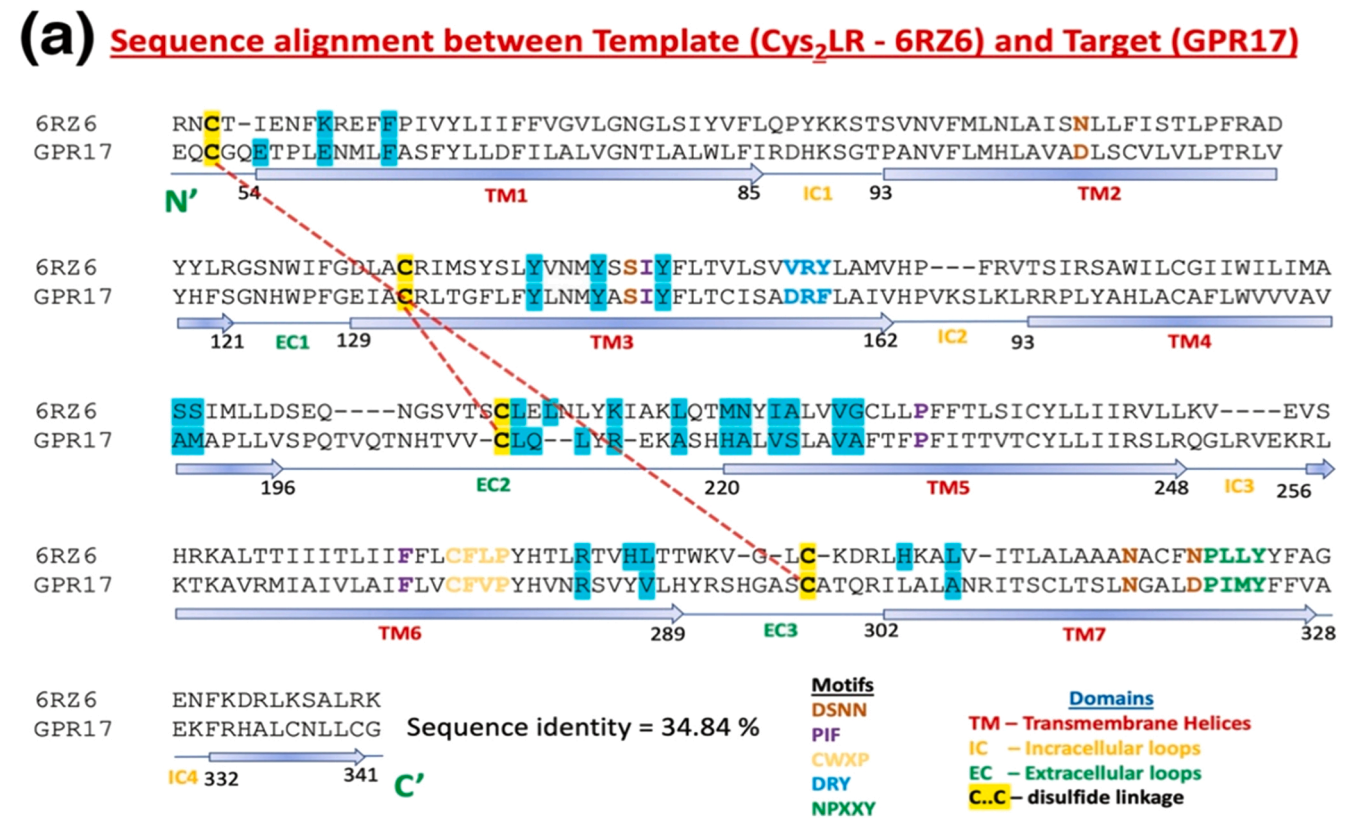

(caption on next page)

Fig. 1. : (a) Sequence alignment between the template (PDB: 6RZ6) and the target (GPR17: UniprotID Q13304) shows (i) conserved -s-s- linkages (pink arrows), (ii) binding site residues (highlighted in cyan) and (iii) functionally important motifs (DSNN, PIF, CWxP, DRY and NPxxY) are properly aligned. The blue arrows indicate TM segments. (b) The structural superposition of the homology model of GPR17 (pink) complexed with x-ray ligand (ONO-2570366; carbon atoms in green VDW) and the template (white, PDBID: 6RZ6). The superposition highlights the proper alignment of the secondary structure regions. Moreover, the x-ray ligand (highlighted in spheres) buried inside the orthosteric binding pocket (sticks representation in pink color), the membrane boundaries such as extracellular (EC), transmembrane (TM), intracellular (IC) and the conserved motifs (highlighted in spheres; DSNN in orange; PIF in purple, CWxP in yellow, DRY in cyan and NPxxY in dark green) are highlighted. (c) The magnified view of the binding site residues shows that the x-ray ligand fits properly inside the pocket. Additionally, the network of polar interactions that stabilizes the complex formation between the surrounding residues of GPR17 and the x-ray ligand were highlighted in yellow dotted lines. (d) The structural superposition of homology-based model (pink) of GPR17 against AlphaFold model (cyan; https://alphafold.ebi.ac.uk/entry/Q13304) shows that the core 7TM regions were highly conserved, while the loop regions from both the EC and IC regions shows lesser deviation, which is negligible. The very-long flanking segments from both N and C terminals were truncated for clarity.

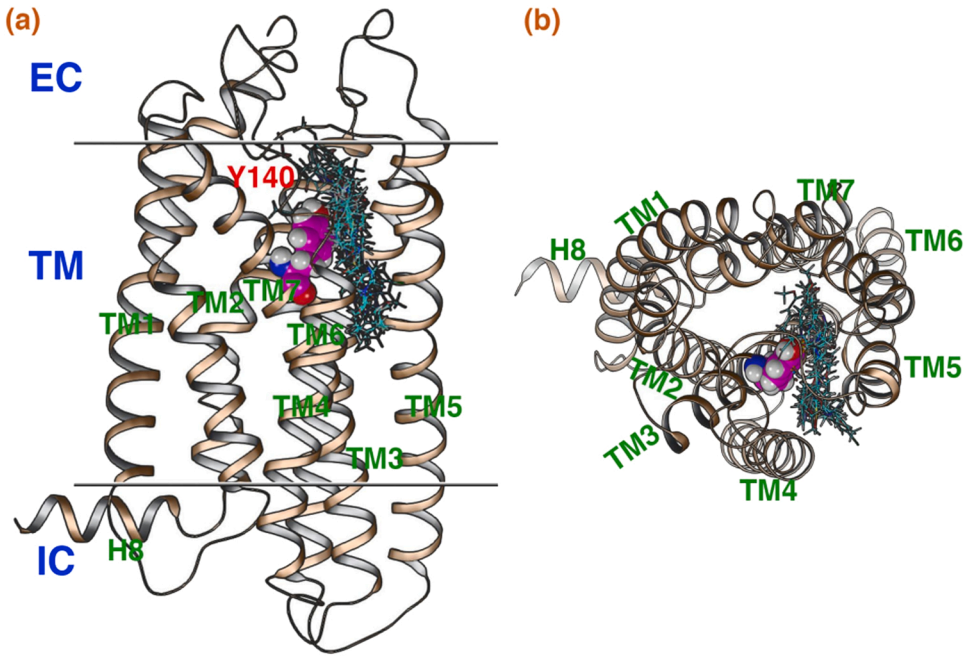

Fig. 2. : The cluster of 17 FDA-approved drugs (cyan in sticks representation) bound to the orthosteric binding pocket of GPR17 (orange in secondary structure representation) using HTVS protocol. The TM regions of GPR17 are displayed in **(a)** side and **(b)** top view are labeled together with the membrane boundaries. The anchoring residue —Y140— responsible for stabilizing the interaction that is located inside the ligand binding pocket of GPR17 is highlighted by CPK representation (pink - carbons, blue - nitrogen, red - oxygen and white - hydrogens).

field. A total of 179 POPC lipids were used to tightly pack the 7TM regions of the GPR17 from both top and bottom leaflets and solvated using the TIP3P solvation model to which the charge of the systems was properly neutralized with NaCl ions. The Gromacs suite was employed to carry out 100 ns unrestrained production run simulations for all 17 complexes. Finally, the structural stability analyses (Supplementary Fig. S1*: RMSD, S2: RMSF and S3: Rg*) were carried out once all the trajectories were carefully processed using Gromacs inbuilt and in-house scripts. Based on the preliminary analysis, the final frames from each complex were collected and used for further investigation.

3.5. Biased-simulations

In order to identify the potential modulator for GPR17, it is essential to categorize the compounds selected based on HTVS protocol with its binding efficiency. Therefore, in this study, the biased-force pulling or steered molecular dynamics simulation (SMD) method was employed. In principle, the SMD simulation has the capacity to mechanically unfold macromolecules composed of repeated folded units [52], pull the ligand through the binding pocket in the membrane channels [53], dissociate the drug or peptide from its bound conformation in a simulation system [50]. During the dissociation process along the chosen reaction coordinate, the SMD simulation will generate several crucial details, such as, *(i)* pathway that the ligand chooses to egress the receptor binding pocket, *(ii)* peak rupture force (F_{max} in pN) profile, *(iii)* number of polar and residual contacts and *(iv)* plausible variations in the interaction pattern over time that can be useful for various investigations. Also, the dissociation time for a ligand can be calculated based on total time (ns) required for the ligand to completely dissociate from the receptors binding pocket and fully solvated. In some cases, these results can also be used as vital information during the novel drug identification process. Besides, in recent years, the SMD simulation method has been widely used in identification of novel potential modulators [54].

The current study is aimed at identifying the novel drugs with significant binding capacity in comparison with other candidates that are obtained from the previous HTVS investigation. For this purpose, the peak rupture forces (F_{max} in pN) obtained from the pulling simulation for all selected HTVS candidates can be used as a valid parameter. Here, to obtain the F_{max}, initially, a range of constant velocities (v) and spring constants (k) were used in our simulations, particularly, on all the selected drugs that are complexed with GPR17. This investigation aided to narrow down towards appropriate force constants that enabled ligand egression progress from the GPR17 binding pocket, i.e., when the higher v and k were applied to the ligand, which created distortion in the simulation systems by causing protein or ligand deformation or unreliable conformations. Therefore, only smaller values (v = 0.003 nm/ps and k = 350 kJ/mol/nm^2) were assigned to these parameters. Also, towards the novel drug identification, these parameters were maintained for all the approved drugs with x-ray compounds together, and 4 ns pulling simulations were carried out, respectively. It was estimated that the pulling simulation time (4 ns) was appropriate for the selected drugs towards complete egress progress.

The force extension curves as a function of simulation time were obtained for all FDA-approved drugs and compared with the xray

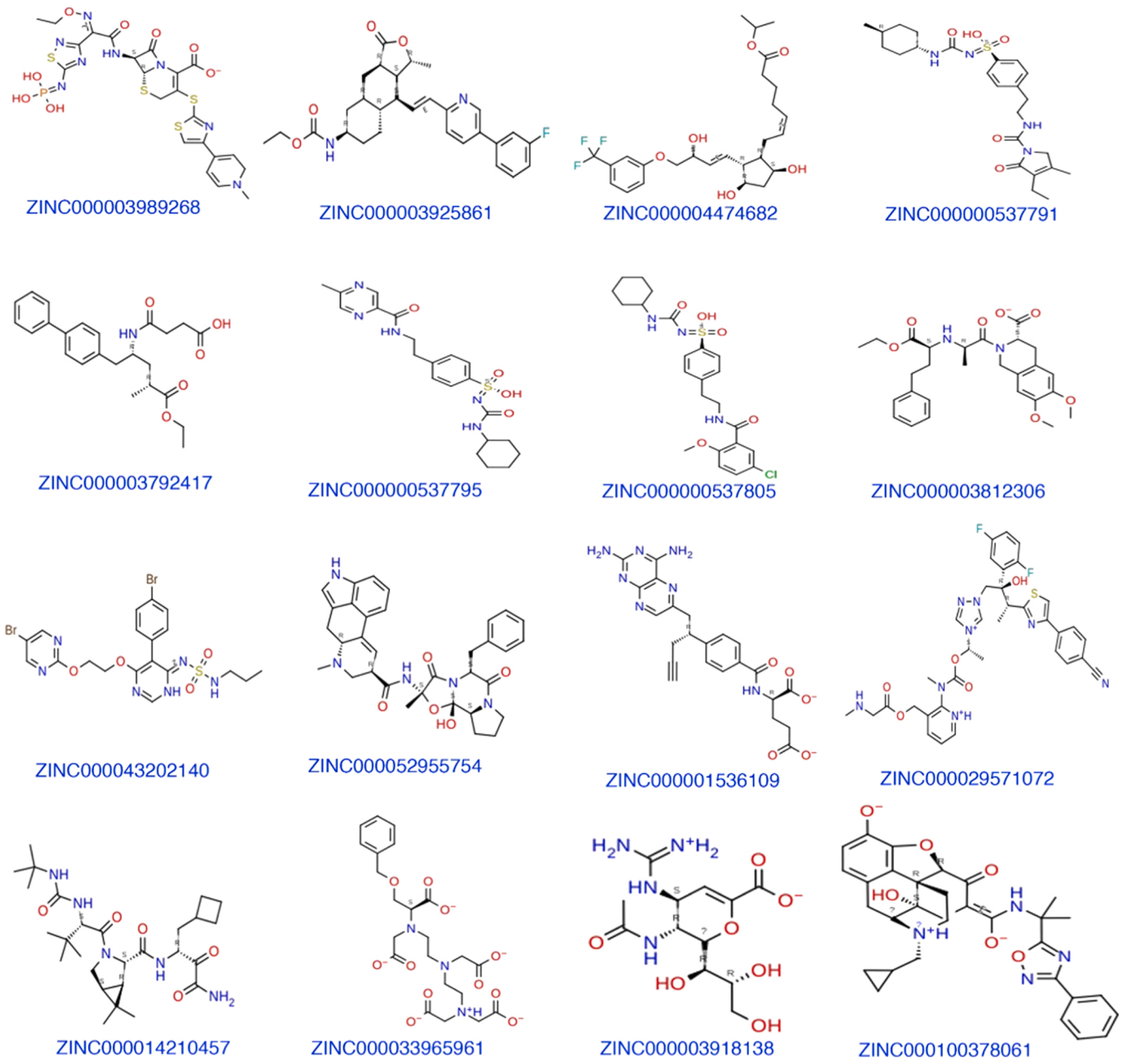

Fig. 3. : Selected top 16 compounds from XP method.

compound (Fig. 5). In the initial stage of the pulling simulation all the drugs were in bound state with GPR17. Subsequently, the bound drug is observed to gradually disengage from the binding pocket and the required time range for all the drugs to completely dissociate from the binding pocket was between 0.75 and 2.2 ns. As the F_{max} acts as a major driving factor for the bound drugs towards breaking all the non-bonded interactions with the surrounding residues, causing eventually to reach a fully solvated state. In addition, the F_{max} peaks for each drug was analyzed. Fig. 5 and Table 2 demonstrates that the pulling simulation applied for the selected hit compounds attained the F_{max} at different time periods and exhibited the peak values ranging from 436.39 pN to 1845.9 pN. Also, during the pulling simulation, each approved drug adopted a unique dissociation pathway to attain the F_{max} peaks. The reason behind this significant variation in F_{max} peaks for the selected hits are due to the diverse chemical moiety of the screened drugs that encountered diverse interaction profiles during the drugs dissociation process.

Moreover, the force profile obtained for the xray compound was used as a benchmark to separate the selected FDA approved compounds into strong and weak binding drugs. Consequently, among the drugs from the strong binding group, the F_{max} values for the top four candidates were alone selected and subjected to the experimental verification (Fig. 6).

3.6. *Intermolecular Polar contacts during pulling simulation*

The polar contacts between the FDA-approved drugs and the residues surrounding the binding pockets of GPR17 are crucial, and act as a major driving force for the complex stability. Therefore, the evolution of total number of polar contacts between each FDA-approved drug, and the binding site residues of GPR17 were computed. The Fig. 7 demonstrates the evolution of the polar contacts only for the top ranked FDA-approved drugs (ZINC000003792417, ZINC000014210457, ZINC000001536109 and ZINC000003925861) that exhibit higher F_{max} values during pulling simulation compared to the other candidates. Also, it appears that the polar interactions are highly variable and fluctuate significantly from

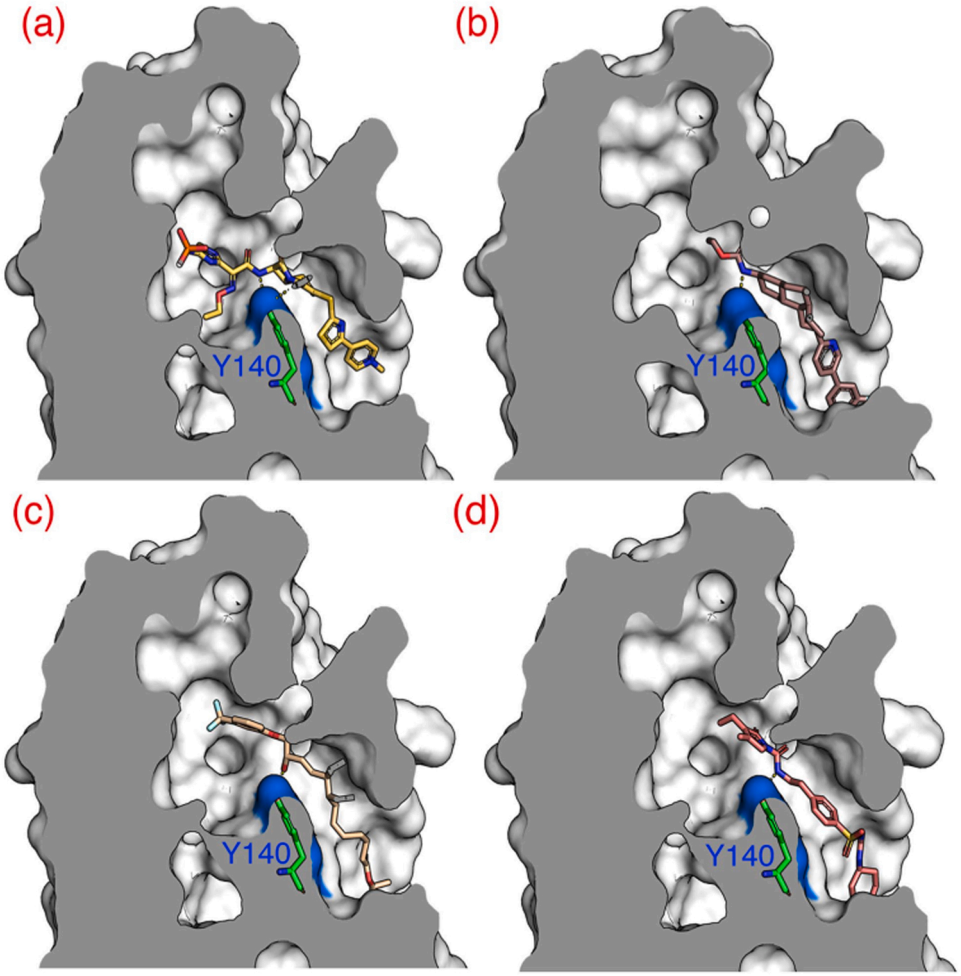

Fig. 4. : The conformational pose of top four FDA-approved drug compounds (a-e: sticks representation) inside the orthosteric binding pocket of GPR17 (slided surface representation) obtained from XP approach. The position of the anchoring residue –Y140– is highlighted in the molecular surface representation (inside: green stick representation) in blue color, which interacts with every FDA-approved drug through polar interaction (yellow dotted lines).

Table 1
List of FDA-approved drug compounds screened with HTVS protocol using Maestro suite. The binding potentials for each drug to GPR17 were initially estimated using Glide (kcal/mol) score and ranked based on prime-MMGBSA (kcal/mol) score. The drug/brand names and its pharmacological profiles for each drug was retrieved from the Drugbank DB (https://go.drugbank.com).

Zinc ID	Drug/Brand name	Pharmacological profile	Glide	MMGBSA
ZINC000003989268	Ceftaroline Fosamil/*Zinforo*	Antibacterial agent.	-11.87	-112.81
ZINC000003925861	Vorapaxar/*Zontivity*	Antithrombotic cardiovascular agent.	-10.97	-90.23
ZINC000004474682	Travoprost/*Duotrav*	To treat elevated intraocular pressure.	-10.20	-87.01
ZINC000000537791	Glimepiride/Amaryl	To treat type 2 diabetes mellitus.	-10.42	-81.12
ZINC000003792417	Sacubitril/*Entresto*	To treat the risk of cardiovascular events.	-10.86	-79.74
ZINC000000537795	Glipizide/*Glucotrol*	To treat low blood glucose.	-9.82	-79.34
ZINC000000537805	Glyburide/Diabetes	To treat diabetes mellitus type II.	-9.11	-74.90
ZINC000003812306	Moexipril/*Univasc*	To treat hypertension.	-8.83	-70.32
ZINC000043202140	Macitentan/Opsumit	To treat pulmonary arterial hypertension.	-8.92	-69.46
ZINC000052955754	Ergotamine/*Cafergot*	To treat migraines.	-10.48	-66.72
ZINC000001536109	Folotyn/Pralatrexate	To treat peripheral T-cell lymphoma.	-9.27	-63.41
ZINC000029571072	Isavuconazonium/Cresemba	Antifungal agent.	-9.79	-55.90
ZINC000014210457	Victrelis/Boceprevir	To treat chronic hepatitis C.	-8.97	-54.08
ZINC000033965961	Gadobenic acid/Multihance	Contrast agent in MRIs.	-10.16	-47.55
ZINC000003918138	Zanamivir/Relenza	To treat influenza A and B.	-8.66	-36.65
ZINC000100378061	Naldemedine/Symproic	To treat opioid-induced constipation.	-9.78	-34.92

the beginning until ~ 2.2 ns time period. The reason behind these differences in Hbond fluctuations between these selected hits are due to differences in chemical moiety. The total number of Hbonds that stabilized the complex formation range between at least 1 to maximum 6 bonds.

The Fig. 7a shows that in the initial stage of the simulation, the ZINC000003792417 drug forms only a negligible number of polar contacts and it continues until 0.8 ns. Later, as the F_{max} applied on the drug escalates, the drug initiates its egression towards EC side of the receptor causing the drug to encounter new surrounding contact

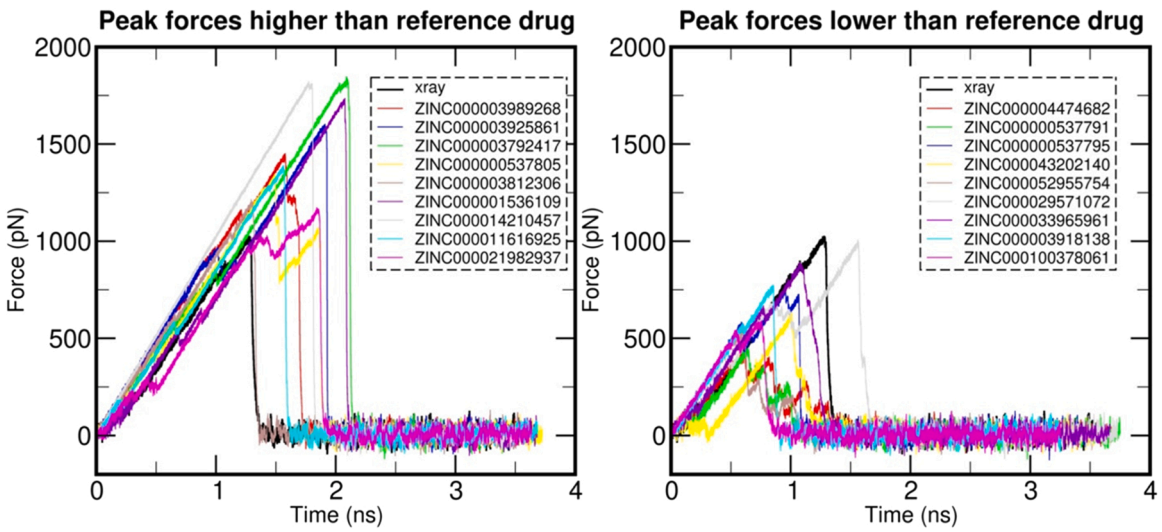

Fig. 5. : The FDA-approved compounds were discerned into **(a)** strong and **(b)** weak binding drugs based on the force profiles (F_{max} in pN) obtained during the pulling simulations. Here, the F_{max} obtained for the x-ray compound was used as the benchmark towards hit selection. A 4 ns simulation was carried out for each selected complex.

Table 2
List of FDA-approved compounds and its peak force (F_{max} in pN) obtained from pulling simulation. The compounds highlighted in asterisk (*) demonstrates higher energies and was subjected to experimental validation.

S.No	Zinc ID	Time (ns)	F_{max} (pN)
1	ZINC000003989268	1.57	1454.70
2	ZINC000003925861	1.91	* 1602.80
3	ZINC000004474682	0.61	436.39
4	ZINC000000537791	0.63	450.06
5	ZINC000003792417	2.08	* 1845.90
6	ZINC000000537795	0.94	754.04
7	ZINC000000537805	1.49	1347.30
8	ZINC000003812306	1.29	1213.32
9	ZINC000043202140	1.00	632.62
10	ZINC000052955754	0.59	571.03
11	ZINC000001536109	2.07	* 1735.20
12	ZINC000029571072	1.56	1005.80
13	ZINC000014210457	1.77	* 1822.10
14	ZINC000033965961	1.07	891.27
15	ZINC000003918138	0.85	774.61
16	ZINC000100378061	0.75	591.09
Xray	xray	1.28	1024.90

residues, and gradual increase in the number of Hbonds (~ 3–4) are observed, which enabled the ligand to maintain this position for a longer period, i.e. from 0.8 to 1.8 ns (~ 1 ns time period). Next, due to further escalation of the applied F_{max}, the drug continued to egress towards EC side of the receptor by breaking the existing stronger Hbond network to create new Hbonds, causing constant reduction in the number of Hbonds (between 1 and 2) than previous phase (1.8–2.2 ns).

The mechanistic investigation during the beginning of the simulation (Fig. 7b; 0.8 ns) shows that the carboxyl group and the O27 atom of the drug established polar contacts with the backbone atoms R214 and H220 residue, respectively. As the force escalates towards the dissociation process, reaching 1.5 ns (Fig. 7c), the drug moved outward leading to the break of the carboxyl group with R214 and establishes new polar interaction with the side chain of Y213, while the N25 and O2 atoms of the drug forms new hydrogen bond (Hbond) interaction with the backbone atoms of R214, respectively. Here, due to an increase in the number of polar contacts, the residues participating in this region might be the secondary interaction site for the drug with the GPR17. Later at 2.1 ns (Fig. 7d), this strong network gets ruptured when the drug moves further outward, but the interaction of N25 atom of the drug with the side chain of Y213 and the O3 atom of the drug with the backbone atom of R214 remain intact, suggesting the importance of Y213 and R214 residues in complex stability which eventually causes the ZINC000003792417 drug to interact with the residues at the upper portion of the binding pocket.

Likewise, the ZINC000014210457 drug also showed an increase in polar contacts during the pulling simulation, but the magnitude of increase is relatively less in comparison with the ZINC000003792417 drug, which demonstrates higher F_{max} value (Fig. 7**e**). Here, as the ZINC000014210457 drug have already established a tight polar network in its native state, ~ 5 Hbonds are observed during the initial period of the simulation. As the F_{max} started to escalate, the Hbond network started to reduce and maintained ~ 3 contacts up until the end of the simulation.

Mechanistically, during the initial phase (Fig. 7f; 0.3 ns), the O12, O32, N34 and O35 atoms of the ZINC000014210457 drug established strong polar interaction with the side chains of Y140, Q199 and R283 residues of GPR17, respectively. After a partial movement of the drug towards EC, the amide group of the drug establishes a polar network with the carboxyl side chain atom of E54, backbone oxygen atom of E49 and nitrogen atom of L212 residues, respectively (Fig. 7g). Additionally, the O32 atom of the drug forms a Hbond with the carboxyl side chain atom of E54 residue. At the final stage (Fig. 7h; 2.1 ns), the drug dissociates further to form multiple Hbond network between the amide groups, i.e., O7, O22 and O32 atoms and the side chain E49, Q50, G52, L210, Q211, L212 and Y213 residues. Overall, polar interaction between the E49 and L212 residues with the ZINC000003925861 drug plays a crucial role in the stability of the complex.

Next, the ZINC000001536109 drug demonstrates the core moiety resembles the classical GPR17 antagonists montelukast and pranlukast [55]. Here, the drug bound to the GPR17 in the alternative binding mode shows ~ 5 polar contacts at the beginning of the pulling simulation. Later, as the drug started the egression due to increase in the F_{max}, it displayed a steady decrease in the number of Hbonds up to ~ 1.8 ns which is followed by a sudden and complete decline, with the total number of Hbonds falling to 0 (Fig. 7**i**). This shows the interactions between the drug and the surrounding residues of GPR17 as intact and remain unchanged over the simulation time. Once the simulation reaches its maximum peak rupture force, all the polar contacts experience sudden rupture which leads to immediate drug egression.

Here, the HTVS docking shows that the drug occupied the binding pocket of GPR17 firmly, by aromatic rings facing inward and the two

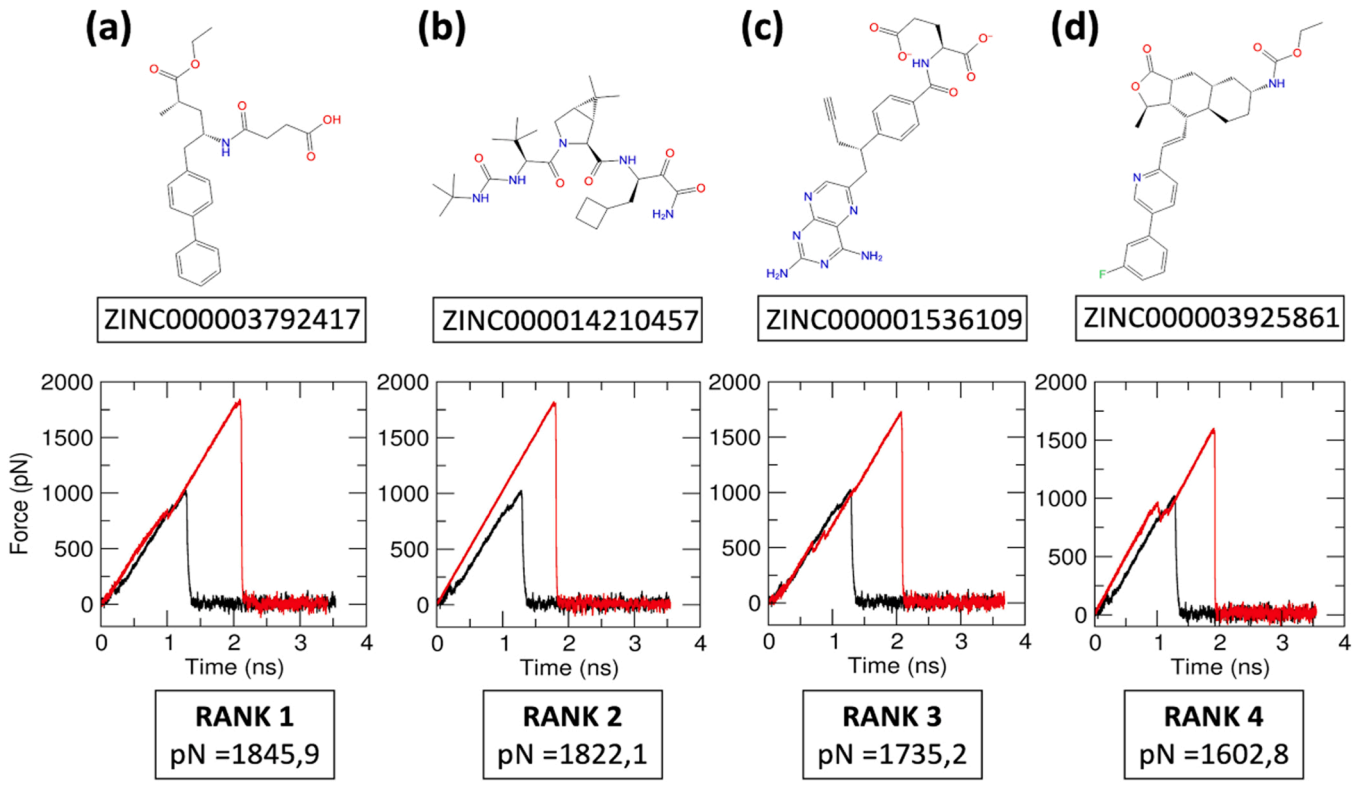

Fig. 6. : The FDA-approved compounds ranked based on peak forces (F_{max} in pN) obtained from pulling simulations.

carboxyl branches facing outward the pocket. Here, the positively charged atoms located in the aromatic rings of the drug and participated in the formation of two polar contacts with Y144 residue, while the double carboxyl group established strong ionic locks with R214 and R263 residues from both sides, respectively (Fig. 7j). As the ionic interactions are energetically stronger than other interactions, the drug remained intact in the same position, all over simulation time (Fig. 7k). Once the simulation reaches the F_{max} which is essential to rupture these strong contacts, the drug eventually flipped out of the pocket immediately. Here, the two arginine residues –R214 and R263 are located on both sides of the pocket play a major role in holding the ZINC000001536109 drug inside the GPR17 binding pocket which is the most energetically favorable conformation.

The Fig. 7l (0.6 ns) demonstrates that in the initial stage of simulation, the ZINC000003925861 drug displays only a negligible number of polar contacts with GPR17. As the simulation evolves towards dissociation of the drug (1.6 ns), the number of polar contacts increases (~ 5 bonds) in comparison with that in the initial time period, suggesting that the chemical nature of the drug detects more favorable interactions, i.e., the secondary interaction site from the surrounding residues of GPR17. Finally, once the simulation reached 1.8 ns, the drug maintained the same number of polar contacts and smoothly executed complete dissociation and attained a fully solvated state.

The graphical investigation reveals that at the beginning of the simulation the drug established a polar contact with the side chain of Y140 (Fig. 7m). Subsequently, the drug dissociates further to establish Hbonds between the side chain S197, side chain and backbone atoms of Q199 and backbone atoms of R214 and the O3, O5, N6 and O19 atoms of the drug, respectively (Fig. 7n). Finally, after rupturing all existing Hbonds, ~ 7 new Hbonds were formed between the P198, T200, V208, Q211, E215 and K216 residues of GPR17 and O3, O5, N6 and O19 atoms of the ZINC000003925861 drug, respectively, to maintain complex stability (Fig. 7o).

The graphical investigation of these trajectories displays that the selected drugs became fully solvated by drifting out from the GPR17 binding pocket during ~ 1.8–2.2 ns of the simulation time. Apart from these polar interactions, the complex stability was further aided by other surrounding residues. Overall, it is worth mentioning that the pulling simulations for the selected drugs out of GPR17 binding pocket is essential in computing the dynamic evolution of the Hbond interaction together with the other aforementioned crucial details that are highly reliable, whereas the other forces used were generated only with unreliable outputs which were incomparable.

3.7. *Influence of the most promising agent towards GPR17 modulation*

Among the top four candidates, the influence of ZINC000003792417 drug towards receptor modulation was explored due to its most promising binding features (higher F_{max} value and longer polar interactions). For this purpose, the initial and the final frames of the GPR17 were extracted from the MD simulation. These frames were then subjected to pairwise superposition which revealed that the RMSD value was 1.7 Å, which gives higher confidence particularly for TM regions.

The graphical investigation reveals that all TM regions overlaps very well with the exception of a segment of TM6 and TM7 (Fig. 8). Also, to understand the helix displacement better, the residues in the helix that showed remarkable differences were picked as probe atoms and its distances were measured.

First, the segments that pose helix displacement on TM6 during MD simulation was closely investigated. Here, the F276 residue which is located at the center of TM6 helix has displaced about 2.7 Å and L257 which is located at the terminal position facing IC side of the helix has displaced about 5.7 Å distance. Overall, this shows that the TM6 has only a moderate effect on the structural deviation within the chosen simulation time.

In contrast, the TM7 helix was closely examined to detect any displaced regions. The investigation displays that the TM7 shows a significant displacement in comparison with the other TM helices. Here, the residues S315, N317 and A319 from 0 ns were measured w.r.t 100 ns, which displays 6.2 Å, 8.3 Å and 5.7 Å deviation, respectively. Overall,

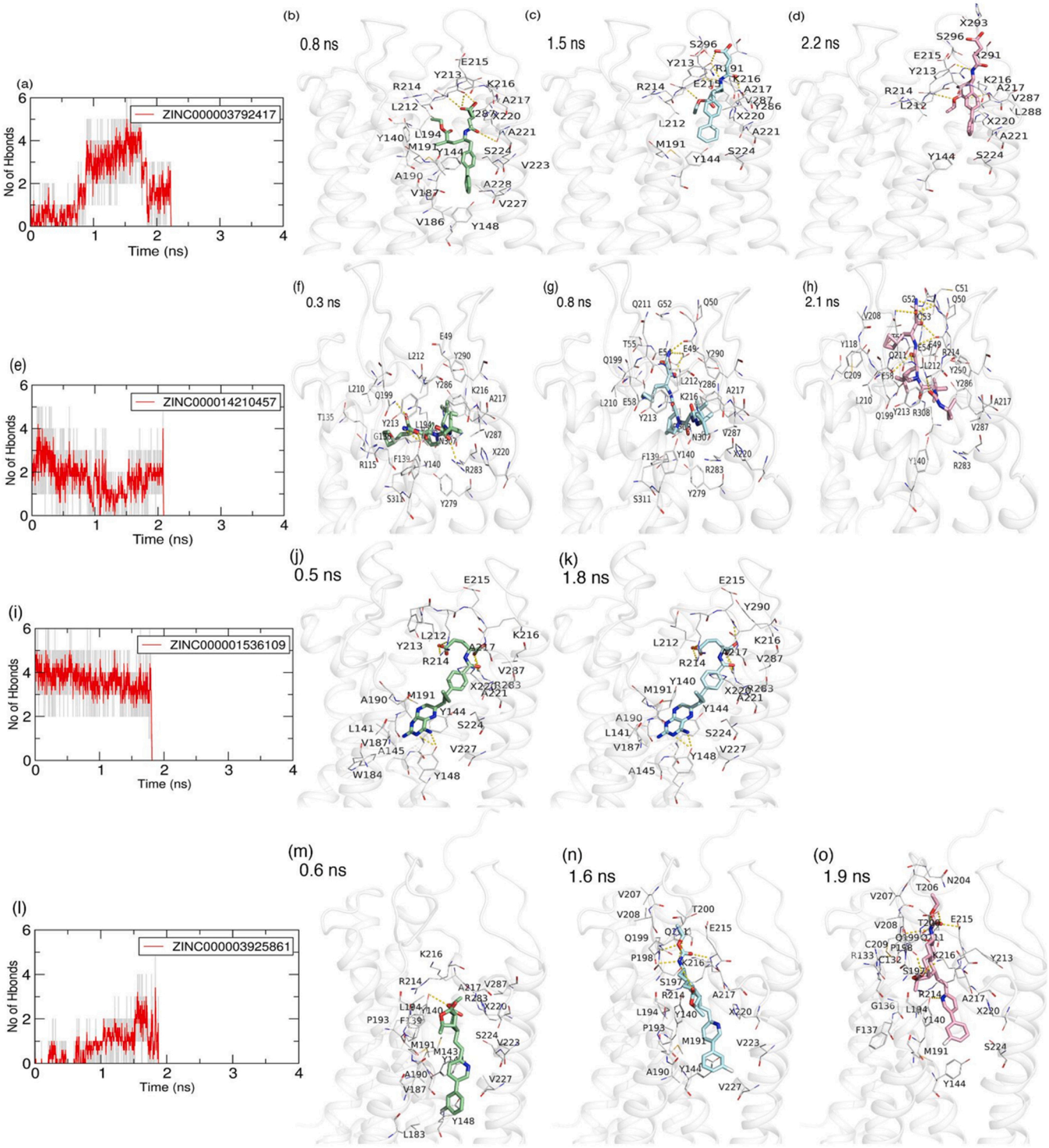

Fig. 7. The total number of Hbond evolution (gray; a,e,i and l) with its average (red) and molecular interaction network depicted for top four FDA-approved drugs –(b-d) ZINC000003792417, (f-g) ZINC000014210457, (j and k) ZINC000001536109 and (m and o) ZINC000003925861– complexed with GPR17 (secondary structure representation highlighted in pale white) during the pulling simulation. The different period of time (ns) based network of polar contacts (yellow dotted lines) highlighting the stepwise dissociation process of the FDA-approved drugs from the GPR17 binding pocket. During the dissociation process, breaking of existing bonds and formation of new polar contacts at different time periods of the simulation are observed. After the final frame for each complex (d, h, k and o), the selected drugs were completely released from the binding pocket and fully solvated (not shown here).

based on the analysis we predict that the ZINC000003792417 drug has significant influence on structural modulation and receptor activation towards the downstream signaling.

3.8. Repurposing drugs to activate GPR17 signaling in GBM cells

The cAMP is an important intracellular second messenger in GPCR signal transduction. The activation $G_{\alpha s}$ protein leads to an increased production of intracellular cAMP levels while it does the opposite with

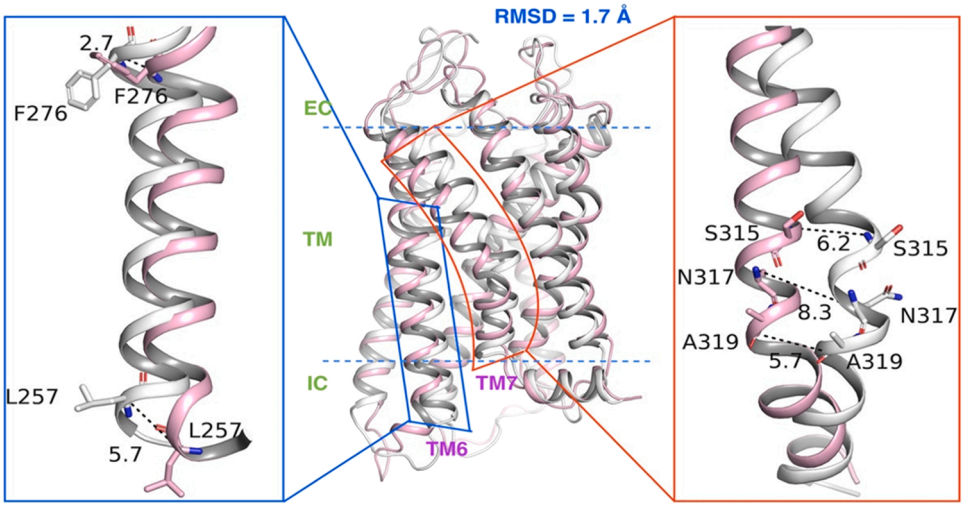

Fig. 8. : Structural superposition of initial (0 ns; white) and final (100 ns; pink) frames from 100 ns MD simulation of GPR17- ZINC000003792417 complex (middle). The magnified image projecting the structural deviation of TM6 (blue box in the left) and TM7 (red box in the right) segments.

$G_{\alpha i}$ protein activation. We used cAMP-Glo Assay (V1501, Promega, USA) as described in method where the measured luminescence is inversely proportional to cAMP levels. Computationally predicted GPR17-targeting top four repurposing drug Vorapaxar, Pralatrexate, Victrelis, and Sacubitirl were tested against GPR17 activation in GBM cells, SNB19 and LN229. The results indicates that increased luminescence over the increased drug concentrations which was interpreted as the activation of $G_{\alpha i}$ which inhibits the adenylate cyclase activity and phosphorylation of protein kinase A (PKA). pEC_{50} of all the four drugs were calculated from the sigmoidal dose-response curve in both cell lines SNB19 and LN229 (Fig. 9). A stimulatory agonist causes an increase in response as the drug concentration increases and inhibitory agonist causes a decreased response as the drug concentration increases. The raw data indicated an increased luminescence with increased concentration which was interpreted as a decreased level of intracellular cAMP. An increase in drug concentration leads to a decline of the intracellular cAMP which proved that Vorapaxar, Pralatrexate, Victrelis, and Sacubitirl can act as a GPR17 agonists via Gαi coupled protein signaling. Fig. 8A shows the responses of novel agonist on LN229 cell lines were the cell treated with Sacubitril showed response with a pEC_{50} of 4.841 while 4.217, 4.406, 4.297 was observed for Vorapaxar, Pralatrexate, Victerlis, respectively. The SNB19 cells treated with drug treated showed the pEC_{50} of 4.661, 3.951, 4.302 and 4.191 for Sacubitril, Vorapaxar, Pralatrexate, Victerlis, respectively (Fig. 8B). Previously, we have shown that the previously well-known agonist, MDL29951 has the pEC_{50} of 4.77 on LN229 cells while 4.75 on SNB19 cells. The data of pEC_{50} suggest that Sacubitril could be a better agonist for GPR17 compared to other drugs tested and also the effect of Sacubitril is almost closer to that of MDL29951.

3.9. Selective binding of repurposing drug with human GPR17

Binding specificity of the novel ligands with GPR17 was also quantified through gene silencing experiments in both GBM cell lines. Fig. 8C shows the cAMP inhibitory effect of the four ligands where the cells treated with siRNA followed by forskolin addition was used as a control. The decreased level of cAMP was observed in control as the luminescence intensities were high in all drug treated conditions. The significant inhibition of cAMP level in siRNA and drug treated condition suggests that these drugs can have a selective binding efficacy with GPR17. As compared to control, all the other samples treated with the new ligands and MDL29951 depicted low level of cAMP. Among them, Sacubitril had a relatively low level of cAMP as compared to MDL 29951 which is also an inhibitory agonist (Fig. 8C). It can be deduced that there is some specific binding of the new ligands to GPR17 receptor as lower level of cAMP was observed due to their inhibitory effects on the cells. However, due to silencing of GPR17, the increased level of intracellular of cAMP was expected after forskolin induction but the agonists activation showed the contrary results that can be justified by the leakiness of GPR17 and inefficient silencing. This data also suggests that Sacubitril may have potential binding specificity with GPR17 compared to other repurposing drugs tested in GBM cells.

4. Conclusion

GBM is recognized as the most aggressive type of cancer which damages the brain cells in adults, and the mortality rate has been reported high which per se indicates low chances of survival. It was determined that GPR17 —the macromolecular target reported to be present on the surface of GBM cell surface— plays one of the central roles to combat against GBM. Therefore, the current study proposes potential modulators that could effectively bind to GPR17 to treat this deadly disease within a short period of time and eventually down-regulate the GBM disease progression.

For this process, the current study has deployed the drug repurposing approach that can reduce failure, huge cost, and time. Although this strategy has been used for decades, this method has acted as a promising alternative for the traditional drug discovery process and has identified several drugs to treat numerous deadly pathologies. Considering that, the multiple computational approaches were used to identify potential drugs from a database of FDA-approved drugs with high-throughput virtual screening approach, after preliminary sequence analysis followed by homology modeling. Later, a subset of approved drugs were identified from our initial investigation, and all the GPR17-drug complexes were immediately subjected to intensive multiscale MD simulations embedded in the POPC membrane. The MD simulations revealed that the selected drugs bind firmly to the orthosteric binding pocket of GPR17 through a number of polar and van der Waals interactions, and at the same time without inducing any major structural changes. Later, a range of external bias-potentials were applied to the bound drug and pulled along the Z axis which is the perpendicular to the membrane plane. The Cα atoms of the GPR17 were restrained in the specific position. The bias-potential aided simulations have generated peak rupture forces and dissociation pathways that are unique for each drug which reflects the diverse chemical moiety of the drugs involved in a distinctive interaction pattern. The peak-forces (pN) enabled to classify the identified drugs as strong and weak binders based on the force obtained from the reference drug (xray). Based on the top peak values, the

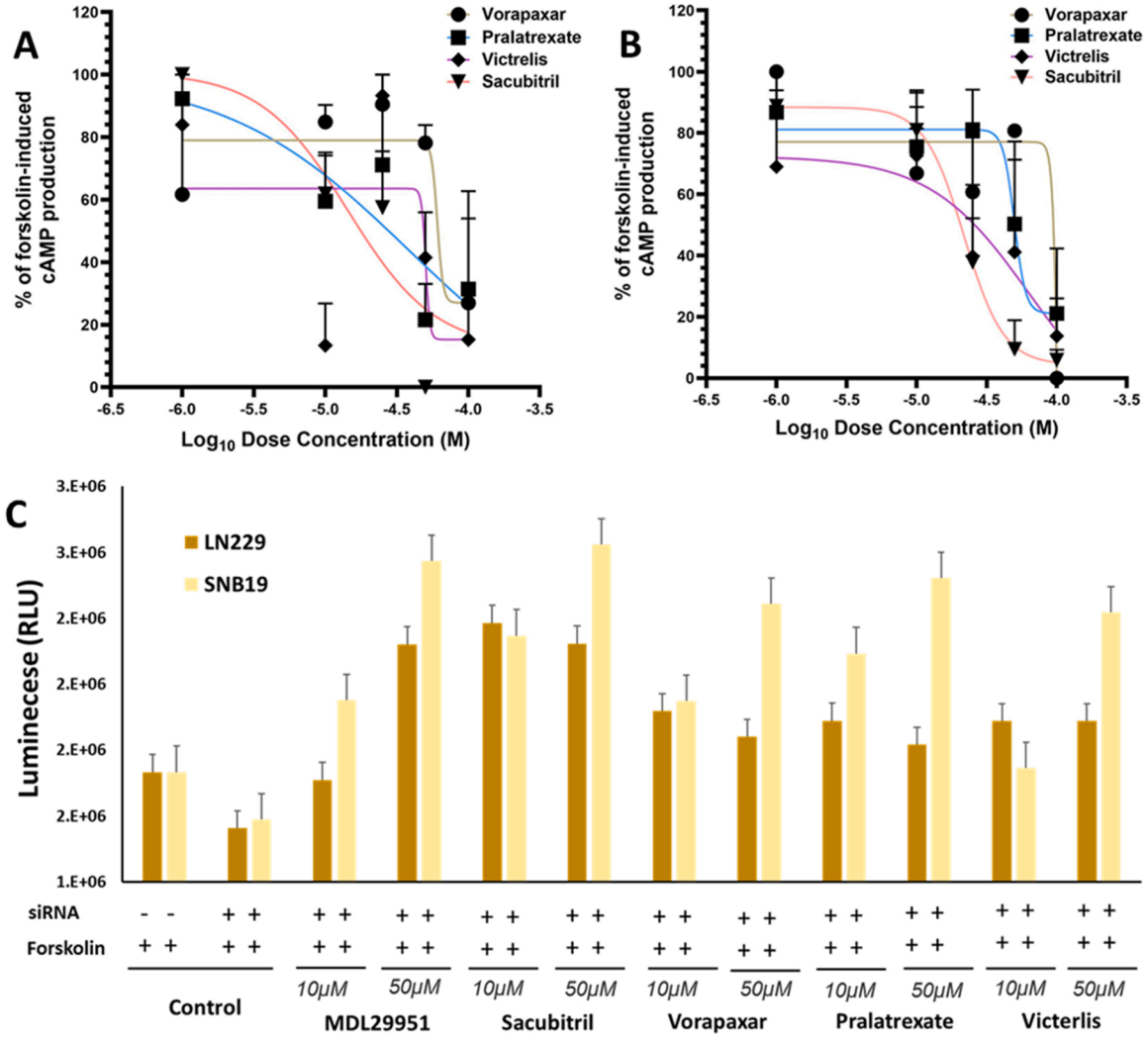

Fig. 9. : Effect of GPR17 agonists on the forskolin-stimulated cAMP accumulation in GBM cells. (A) Agonism of Vorapaxar, Pralatrexate, Victrelis, and Sacubitirl with human GPR17 inhibits intracellular cAMP over the concentrations in LN229 and (B) in SNB19 cells. For each antagonist, pEC_{50} values are reported. Each point is expressed as a percentage of normalized cAMP inhibition set to 100% and is the mean±S.E.M. of biological and technical repeats. Data analysis was performed with GraphPad Prism® software, version 4.02, for Windows® using a sigmoidal dose-response equation. (C) Cells were treated with the indicated amount of agonist MDL29,951, Vorapaxar, Pralatrexate, Victrelis, and Sacubitirl. In the negative control cells were treated with forskolin and without siRNA. In the positive control alone cells were treated with both siRNA and forskolin. Each point represents three data points; the error bars represent the mean±S.E.M.

ZINC000003792417, ZINC000014210457, ZINC000001536109 and ZINC000003925861 drugs were identified as the top hits. The pulling simulations revealed that the polar interactions between the drug-receptor complexes play a vital role in the complex formation. Additionally, the hot spot residues (residues involved in long-period polar interaction with the drugs) for the selected drugs were also elucidated. In this research, we have used GBM cell lines, LN229 and SNB19, that over express GPR17 protein endogenously. Activation of GPR17 signaling with the identified repurposing drugs have inhibited the cAMP formation in GBM cells. Our data suggest that GPR17 specific drug repurposing might suppress the proliferation of GBM cells in vivo, a targeted therapy regulated by GPR17 signaling pathway. Considering the side effects of existing chemotherapeutic agents, identified repurposing drugs might represent a promising treatment modality for GBM patients. The availability of existing clinical data of the identified FDA approved drugs might also provide therapeutic opportunities for treating glioblastoma in the future. Overall, the drugs that were identified in the current study might act as the most promising inhibitors towards GBM downregulation, which require further experimental validation. Additionally, the details obtained from the current investigation would significantly improve the overall prospects of developing therapeutic agents to impede GBM progression.

CRediT authorship contribution statement

SK and AM performed biochemical assays, in-vitro studies and data analysis. PM and J.R performed all in silico analysis. MK, SK, PM and TR managed all studies. MK and PM conceived the project. All the authors contributed to writing the manuscript.

Conflict of interest statement

The authors declare no conflict of interest.

Acknowledgments

P.M. gratefully acknowledges the use of the bioinformatics infrastructure facility supported by Biocenter Finland, grants from the Joe, Pentti and Tor Borg Memorial Fund 2021, the Sigrid Juselius Foundation and the CSC-IT Center for Science (Project: 2000461) for the

computational facility; Dr. Jukka Lehtonen for the IT support; Prof. Outi Salo-Ahen (Pharmacy) Åbo Akademi University, Pharmacy for providing the lab support. J.R. gratefully acknowledge financial support from the Ministry of Innovative Development of the Republic of Uzbekistan (Project: AL36-2105821C). M.S.K. would like to thank Kirsi Rautajoki for the kind gift of GBM cell lines, Tampere University, Finland. P.M. gratefully acknowledges the APC support by ÅAU APC pool 2022.

Appendix A. Supporting information

Supplementary data associated with this article can be found in the online version at doi:10.1016/j.biopha.2023.114320.

References

[1] Y. Chen, et al., The oligodendrocyte-specific G protein-coupled receptor GPR17 is a cell-intrinsic timer of myelination, Nat. Neurosci. 12 (11) (2009) 1398–1406.
[2] K. Simon, et al., The orphan G protein-coupled receptor GPR17 negatively regulates oligodendrocyte differentiation via Gαi/o and its downstream effector molecules, J. Biol. Chem. 291 (2) (2016) 705–718.
[3] K.M. Saravanan, et al., Identification of novel GPR17-agonists by structural bioinformatics and signaling activation, Int J. Biol. Macromol. 106 (2018) 901–907.
[4] P.P. Mehta, V.S. Dhapte-Pawar, Repurposing drug molecules for new pulmonary therapeutic interventions, Drug Deliv. Transl. Res. 11 (5) (2021) 1829–1848.
[5] V. Parvathaneni, et al., Drug repurposing: a promising tool to accelerate the drug discovery process, Drug Discov. Today 24 (10) (2019) 2076–2085.
[6] C. Ma, et al., Boceprevir, GC-376, and calpain inhibitors II, XII inhibit SARS-CoV-2 viral replication by targeting the viral main protease, Cell Res. 30 (8) (2020) 678–692.
[7] M.A. Martinez, Efficacy of repurposed antiviral drugs: Lessons from COVID-19, Drug Discov. Today 27 (7) (2022) 1954–1960.
[8] D.K. Ngan, et al., Repurposing drugs as COVID-19 therapies: a toxicity evaluation, Drug Discov. Today 27 (7) (2022) 1983–1993.
[9] B. Huang, Y. Zhang, Teaching an old dog new tricks: drug discovery by repositioning natural products and their derivatives, Drug Discov. Today 27 (7) (2022) 1936–1944.
[10] M. Liao, et al., Small-molecule drug discovery in triple negative breast cancer: current situation and future directions, J. Med. Chem. 64 (5) (2021) 2382–2418.
[11] A. Lakizadeh, S.M. Hassan Mir-Ashrafi, *Drug repurposing improvement using a novel data integration framework based on the drug side effect*, Inform. Med. 23 (2021), 100523.
[12] C. Fetro, D. Scherman, Drug repurposing in rare diseases: myths and reality, Therapie 75 (2) (2020) 157–160.
[13] E. Athanasiadis, Z. Cournia, G. Spyrou, ChemBioServer: a web-based pipeline for filtering, clustering and visualization of chemical compounds used in drug discovery, Bioinformatics 28 (22) (2012) 3002–3003.
[14] E. Sam, P. Athri, Web-based drug repurposing tools: a survey, Brief. Bioinform. 20 (1) (2019) 299–316.
[15] E. Karatzas, et al., ChemBioServer 2.0: an advanced web server for filtering, clustering and networking of chemical compounds facilitating both drug discovery and repurposing, Bioinformatics 36 (8) (2020) 2602–2604.
[16] A. Tuerkova, B. Zdrazil, A ligand-based computational drug repurposing pipeline using KNIME and programmatic data access: case studies for rare diseases and COVID-19, J. Chemin. 12 (2020) 71.
[17] G. Fiscon, P. Paci, SAveRUNNER: an R-based tool for drug repurposing, BMC Bioinform. 22 (1) (2021) 150.
[18] N. Fosu-Mensah, et al., Advances in small-molecule drug discovery for triple-negative breast cancer, Future Med. Chem. 7 (15) (2015) 2019–2039.
[19] M.A. Farha, E.D. Brown, Drug repurposing for antimicrobial discovery, Nat. Microbiol. 4 (4) (2019) 565–577.
[20] M. Hosseini, et al., Computational molecular docking and virtual screening revealed promising SARS-CoV-2 drugs, Precis. Clin. Med. 4 (1) (2021) 1–16.
[21] P. Marimuthu, S. Gorle, K.R. Karnati, Mechanistic insights into SARS-CoV-2 main protease inhibition reveals hotspot residues, J. Chem. Inf. Model. 61 (12) (2021) 6053–6065.
[22] A.P. Challa, et al., Human and machine intelligence together drive drug repurposing in rare diseases, Front. Genet. 12 (2021), 707836.
[23] C. Choudhury, N. Arul Murugan, U.D. Priyakumar, Structure-based drug repurposing: traditional and advanced AI/mL-aided methods, Drug Discov. Today 27 (7) (2022) 1847–1861.
[24] K. Hatzimouratidis, Sildenafil in the treatment of erectile dysfunction: an overview of the clinical evidence, Clin. Inter. Aging 1 (4) (2006) 403–414.
[25] N. Merten, et al., Repurposing HAMI3379 to block GPR17 and promote rodent and human oligodendrocyte differentiation, Cell Chem. Biol. 25 (6) (2018) 775–786, e5.
[26] D. Morselli Gysi, et al., Network medicine framework for identifying drug-repurposing opportunities for COVID-19, Proc. Natl. Acad. Sci. U.S.A. 118 (2021) 19.
[27] S. van den Berg, et al., Drug repurposing for rare diseases: a role for academia, Front. Pharmacol. 12 (2021), 746987.
[28] R. Sakate, T. Kimura, Drug repositioning trends in rare and intractable diseases, Drug Discov. Today 27 (7) (2022) 1789–1795.
[29] F. Ye, et al., Cryo-EM structure of G-protein-coupled receptor GPR17 in complex with inhibitory G protein, MedComm 3 (4) (2022), e159.
[30] C. UniProt, *UniProt: a hub for protein information*, Nucleic Acids Res. (2015) D204–D212.
[31] G.M. Boratyn, et al., BLAST: a more efficient report with usability improvements, Nucleic Acids Res 41 (2013) W29–W33 (Web Server issue).
[32] F. Sievers, et al., Fast, scalable generation of high-quality protein multiple sequence alignments using clustal omega, Mol. Syst. Biol. 7 (2011) 539.
[33] P.V. Troshin, J.B. Procter, G.J. Barton, Java bioinformatics analysis web services for multiple sequence alignment–JABAWS:MSA, Bioinformatics 27 (14) (2011) 2001–2002.
[34] P.V. Troshin, et al., JABAWS 2.2 distributed web services for bioinformatics: protein disorder, conservation and RNA secondary structure, Bioinformatics 34 (11) (2018) 1939–1940.
[35] B. Webb, A. Sali, Comparative protein structure modeling using MODELLER, Curr. Protoc. Bioinform. 54 (2016) 5 6 1–5 6 37.
[36] A. Gusach, et al., Structural basis of ligand selectivity and disease mutations in cysteinyl leukotriene receptors, Nat. Commun. 10 (1) (2019) 5573.
[37] C. Lu, et al., OPLS4: improving force field accuracy on challenging regimes of chemical space, J. Chem. Theory Comput. 17 (7) (2021) 4291–4300.
[38] J.C. Shelley, et al., Epik: a software program for pK(a) prediction and protonation state generation for drug-like molecules, J. Comput. Aided Mol. Des. 21 (12) (2007) 681–691.
[39] J.R. Greenwood, et al., Towards the comprehensive, rapid, and accurate prediction of the favorable tautomeric states of drug-like molecules in aqueous solution, J. Comput. Aided Mol. Des. 24 (6–7) (2010) 591–604.
[40] R. Sankhe, et al., Repurposing of existing FDA approved drugs for Neprilysin inhibition: an in-silico study, J. Mol. Struct. 1224 (2021), 129073.
[41] M.P. Jacobson, et al., A hierarchical approach to all-atom protein loop prediction, Protein.: Struct., Funct., Bioinforma. 55 (2) (2004) 351–367.
[42] E.L. Wu, et al., CHARMM-GUI Membrane Builder toward realistic biological membrane simulations, J. Comput. Chem. 35 (27) (2014) 1997–2004.
[43] J. Huang, et al., CHARMM36m: an improved force field for folded and intrinsically disordered proteins, Nat. Methods 14 (1) (2017) 71–73.
[44] W.L. Jorgensen, et al., Comparison of simple potential functions for simulating liquid water, J. Chem. Phys. 79 (2) (1983) 926–935.
[45] M.J. Abraham, et al., GROMACS: High performance molecular simulations through multi-level parallelism from laptops to supercomputers, SoftwareX 1–2 (2015) 19–25.
[46] T. Darden, D. York, L. Pedersen, Particle Mesh Ewald - an N.Log(N) method for Ewald Sums in large systems, J. Chem. Phys. 98 (12) (1993) 10089–10092.
[47] G. Bussi, D. Donadio, M. Parrinello, Canonical sampling through velocity rescaling, J. Chem. Phys. 126 (1) (2007), 014101.
[48] M. Parrinello, A. Rahman, Polymorphic transitions in single crystals: a new molecular dynamics method, J. Appl. Phys. 52 (1981) 7182–7190.
[49] B. Hess, P-LINCS: a parallel linear constraint solver for molecular simulation, J. Chem. Theory Comput. 4 (1) (2008) 116–122.
[50] P. Marimuthu, J. Razzokov, G. Eshonqulov, Disruption of conserved polar interactions causes a sequential release of Bim mutants from the canonical binding groove of Mcl1, Int. J. Biol. Macromol. (2020).
[51] W. Humphrey, A. Dalke, K. Schulten, VMD: visual molecular dynamics, J. Mol. Graph 14 (1) (1996) 33–38, 27-8.
[52] J. Razzokov, M. Yusupov, A. Bogaerts, Oxidation destabilizes toxic amyloid beta peptide aggregation, Sci. Rep. 9 (1) (2019) 5476.
[53] B. van den Berg, et al., Structural basis for silicic acid uptake by higher plants, J. Mol. Biol. 433 (21) (2021), 167226.
[54] W. Acevedo, F. Gonzalez-Nilo, E. Agosin, Docking and molecular dynamics of steviol glycoside-human bitter receptor interactions, J. Agric. Food Chem. (2016).
[55] G. Marucci, et al., The G protein-coupled receptor GPR17: overview and update, ChemMedChem 11 (23) (2016) 2567–2574.